DESY–02–064

Measurement of high-Q^2 charged current cross sections in e^-p deep inelastic scattering at HERA

ZEUS Collaboration

Abstract

Cross sections for e^-p charged current deep inelastic scattering have been measured at a centre-of-mass energy of 318 GeV with an integrated luminosity of 16.4 pb^{-1} using the ZEUS detector at HERA. Differential cross-sections $d\sigma/dQ^2$, $d\sigma/dx$ and $d\sigma/dy$ are presented for $Q^2 > 200\,\mathrm{GeV}^2$. In addition, $d^2\sigma/dxdQ^2$ was measured in the kinematic range $280\,\mathrm{GeV}^2 < Q^2 < 30\,000\,\mathrm{GeV}^2$ and $0.015 < x < 0.42$. The predictions of the Standard Model agree well with the measured cross sections. The mass of the W boson, determined from a fit to $d\sigma/dQ^2$, is $M_W = 80.3 \pm 2.1\,(\mathrm{stat.}) \pm 1.2\,(\mathrm{syst.}) \pm 1.0\,(\mathrm{PDF})$ GeV.

The ZEUS Collaboration

S. Chekanov, D. Krakauer, S. Magill, B. Musgrave, J. Repond, R. Yoshida
Argonne National Laboratory, Argonne, Illinois 60439-4815 [n]

M.C.K. Mattingly
Andrews University, Berrien Springs, Michigan 49104-0380

P. Antonioli, G. Bari, M. Basile, L. Bellagamba, D. Boscherini, A. Bruni, G. Bruni, G. Cara Romeo, L. Cifarelli, F. Cindolo, A. Contin, M. Corradi, S. De Pasquale, P. Giusti, G. Iacobucci, G. Levi, A. Margotti, R. Nania, F. Palmonari, A. Pesci, G. Sartorelli, A. Zichichi
University and INFN Bologna, Bologna, Italy [e]

G. Aghuzumtsyan, D. Bartsch, I. Brock, J. Crittenden[1], S. Goers, H. Hartmann, E. Hilger, P. Irrgang, H.-P. Jakob, A. Kappes, U.F. Katz[2], R. Kerger[3], O. Kind, E. Paul, J. Rautenberg[4], R. Renner, H. Schnurbusch, A. Stifutkin, J. Tandler, K.C. Voss, A. Weber
Physikalisches Institut der Universität Bonn, Bonn, Germany [b]

D.S. Bailey[5], N.H. Brook[5], J.E. Cole, B. Foster, G.P. Heath, H.F. Heath, S. Robins, E. Rodrigues[6], J. Scott, R.J. Tapper, M. Wing
H.H. Wills Physics Laboratory, University of Bristol, Bristol, United Kingdom [m]

M. Capua, A. Mastroberardino, M. Schioppa, G. Susinno
Calabria University, Physics Department and INFN, Cosenza, Italy [e]

J.Y. Kim, Y.K. Kim, J.H. Lee, I.T. Lim, M.Y. Pac[7]
Chonnam National University, Kwangju, Korea [g]

A. Caldwell, M. Helbich, X. Liu, B. Mellado, S. Paganis, W.B. Schmidke, F. Sciulli
Nevis Laboratories, Columbia University, Irvington on Hudson, New York 10027 [o]

J. Chwastowski, A. Eskreys, J. Figiel, K. Olkiewicz, M.B. Przybycień[8], P. Stopa, L. Zawiejski
Institute of Nuclear Physics, Cracow, Poland [i]

L. Adamczyk, B. Bednarek, I. Grabowska-Bold, K. Jeleń, D. Kisielewska, A.M. Kowal, M. Kowal, T. Kowalski, B. Mindur, M. Przybycień, E. Rulikowska-Zarębska, L. Suszycki, D. Szuba, J. Szuba[9]
Faculty of Physics and Nuclear Techniques, University of Mining and Metallurgy, Cracow, Poland [p]

A. Kotański[10], W. Słomiński[11]
Department of Physics, Jagellonian University, Cracow, Poland

L.A.T. Bauerdick[12], U. Behrens, K. Borras, V. Chiochia, D. Dannheim, M. Derrick[13], G. Drews, J. Fourletova, A. Fox-Murphy, U. Fricke, A. Geiser, F. Goebel[14], P. Göttlicher[15], O. Gutsche, T. Haas, W. Hain, G.F. Hartner, S. Hillert, U. Kötz, H. Kowalski[16], H. Labes, D. Lelas, B. Löhr, R. Mankel, M. Martínez[12], M. Moritz, D. Notz, I.-A. Pellmann, M.C. Petrucci, A. Polini, A. Raval, U. Schneekloth, F. Selonke[17], B. Surrow[18], H. Wessoleck, R. Wichmann[19], G. Wolf, C. Youngman, W. Zeuner
Deutsches Elektronen-Synchrotron DESY, Hamburg, Germany

A. Lopez-Duran Viani[20], A. Meyer, S. Schlenstedt
DESY Zeuthen, Zeuthen, Germany

G. Barbagli, E. Gallo, C. Genta, P. G. Pelfer
University and INFN, Florence, Italy [e]

A. Bamberger, A. Benen, N. Coppola, H. Raach
Fakultät für Physik der Universität Freiburg i.Br., Freiburg i.Br., Germany [b]

M. Bell, P.J. Bussey, A.T. Doyle, C. Glasman, S. Hanlon, S.W. Lee, A. Lupi, G.J. McCance, D.H. Saxon, I.O. Skillicorn
Department of Physics and Astronomy, University of Glasgow, Glasgow, United Kingdom [m]

I. Gialas
Department of Engineering in Management and Finance, Univ. of Aegean, Greece

B. Bodmann, T. Carli, U. Holm, K. Klimek, N. Krumnack, E. Lohrmann, M. Milite, H. Salehi, S. Stonjek[21], K. Wick, A. Ziegler, Ar. Ziegler
Hamburg University, Institute of Exp. Physics, Hamburg, Germany [b]

C. Collins-Tooth, C. Foudas, R. Gonçalo[6], K.R. Long, F. Metlica, D.B. Miller, A.D. Tapper, R. Walker
Imperial College London, High Energy Nuclear Physics Group, London, United Kingdom [m]

P. Cloth, D. Filges
Forschungszentrum Jülich, Institut für Kernphysik, Jülich, Germany

M. Kuze, K. Nagano, K. Tokushuku[22], S. Yamada, Y. Yamazaki
Institute of Particle and Nuclear Studies, KEK, Tsukuba, Japan [f]

A.N. Barakbaev, E.G. Boos, N.S. Pokrovskiy, B.O. Zhautykov
Institute of Physics and Technology of Ministry of Education and Science of Kazakhstan, Almaty, Kazakhstan

H. Lim, D. Son
Kyungpook National University, Taegu, Korea [g]

F. Barreiro, O. González, L. Labarga, J. del Peso, I. Redondo[23], J. Terrón, M. Vázquez
Departamento de Física Teórica, Universidad Autónoma Madrid,Madrid, Spain [l]

M. Barbi, A. Bertolin, F. Corriveau, A. Ochs, S. Padhi, D.G. Stairs, M. St-Laurent
Department of Physics, McGill University, Montréal, Québec, Canada H3A 2T8 [a]

T. Tsurugai
Meiji Gakuin University, Faculty of General Education, Yokohama, Japan

A. Antonov, V. Bashkirov[24], P. Danilov, B.A. Dolgoshein, D. Gladkov, V. Sosnovtsev, S. Suchkov
Moscow Engineering Physics Institute, Moscow, Russia [j]

R.K. Dementiev, P.F. Ermolov, Yu.A. Golubkov, I.I. Katkov, L.A. Khein, I.A. Korzhavina, V.A. Kuzmin, B.B. Levchenko, O.Yu. Lukina, A.S. Proskuryakov, L.M. Shcheglova, N.N. Vlasov, S.A. Zotkin
Moscow State University, Institute of Nuclear Physics, Moscow, Russia [k]

C. Bokel, J. Engelen, S. Grijpink, E. Koffeman, P. Kooijman, E. Maddox, A. Pellegrino, S. Schagen, E. Tassi, H. Tiecke, N. Tuning, J.J. Velthuis, L. Wiggers, E. de Wolf
NIKHEF and University of Amsterdam, Amsterdam, Netherlands [h]

N. Brümmer, B. Bylsma, L.S. Durkin, J. Gilmore, C.M. Ginsburg, C.L. Kim, T.Y. Ling
Physics Department, Ohio State University, Columbus, Ohio 43210 [n]

S. Boogert, A.M. Cooper-Sarkar, R.C.E. Devenish, J. Ferrando, G. Grzelak, T. Matsushita, M. Rigby, O. Ruske[25], M.R. Sutton, R. Walczak
Department of Physics, University of Oxford, Oxford United Kingdom [m]

R. Brugnera, R. Carlin, F. Dal Corso, S. Dusini, A. Garfagnini, S. Limentani, A. Longhin, A. Parenti, M. Posocco, L. Stanco, M. Turcato
Dipartimento di Fisica dell' Università and INFN, Padova, Italy [e]

E.A. Heaphy, B.Y. Oh, P.R.B. Saull[26], J.J. Whitmore[27]
Department of Physics, Pennsylvania State University, University Park, Pennsylvania 16802 [o]

Y. Iga
Polytechnic University, Sagamihara, Japan [f]

G. D'Agostini, G. Marini, A. Nigro
Dipartimento di Fisica, Università 'La Sapienza' and INFN, Rome, Italy [e]

C. Cormack, J.C. Hart, N.A. McCubbin
Rutherford Appleton Laboratory, Chilton, Didcot, Oxon, United Kingdom [m]

C. Heusch
University of California, Santa Cruz, California 95064 [n]

I.H. Park
Seoul National University, Seoul, Korea

N. Pavel
Fachbereich Physik der Universität-Gesamthochschule Siegen, Germany

H. Abramowicz, S. Dagan, A. Gabareen, S. Kananov, A. Kreisel, A. Levy
Raymond and Beverly Sackler Faculty of Exact Sciences, School of Physics, Tel-Aviv University, Tel-Aviv, Israel [d]

T. Abe, T. Fusayasu, T. Kohno, K. Umemori, T. Yamashita
Department of Physics, University of Tokyo, Tokyo, Japan [f]

R. Hamatsu, T. Hirose[17], M. Inuzuka, S. Kitamura[28], K. Matsuzawa, T. Nishimura
Tokyo Metropolitan University, Deptartment of Physics, Tokyo, Japan [f]

M. Arneodo[29], N. Cartiglia, R. Cirio, M. Costa, M.I. Ferrero, S. Maselli, V. Monaco, C. Peroni, M. Ruspa, R. Sacchi, A. Solano, A. Staiano
Università di Torino, Dipartimento di Fisica Sperimentale and INFN, Torino, Italy [e]

R. Galea, T. Koop, G.M. Levman, J.F. Martin, A. Mirea, A. Sabetfakhri
Department of Physics, University of Toronto, Toronto, Ontario, Canada M5S 1A7 [a]

J.M. Butterworth, C. Gwenlan, R. Hall-Wilton, T.W. Jones, J.B. Lane, M.S. Lightwood, J.H. Loizides[30], B.J. West
Physics and Astronomy Department, University College London, London, United Kingdom [m]

J. Ciborowski[31], R. Ciesielski[32], R.J. Nowak, J.M. Pawlak, B. Smalska[33], J. Sztuk[34], T. Tymieniecka[35], A. Ukleja[35], J. Ukleja, J.A. Zakrzewski, A.F. Żarnecki
Warsaw University, Institute of Experimental Physics, Warsaw, Poland [q]

M. Adamus, P. Plucinski
Institute for Nuclear Studies, Warsaw, Poland [q]

Y. Eisenberg, L.K. Gladilin[36], D. Hochman, U. Karshon
Department of Particle Physics, Weizmann Institute, Rehovot, Israel [c]

D. Kçira, S. Lammers, L. Li, D.D. Reeder, A.A. Savin, W.H. Smith
Department of Physics, University of Wisconsin, Madison, Wisconsin 53706 [n]

A. Deshpande, S. Dhawan, V.W. Hughes, P.B. Straub
Department of Physics, Yale University, New Haven, Connecticut 06520-8121 [n]

S. Bhadra, C.D. Catterall, S. Fourletov, S. Menary, M. Soares, J. Standage
Department of Physics, York University, Ontario, Canada M3J 1P3 [a]

[1] now at Cornell University, Ithaca/NY, USA
[2] on leave of absence at University of Erlangen-Nürnberg, Germany
[3] now at Ministère de la Culture, de L'Enseignement Supérieur et de la Recherche, Luxembourg
[4] supported by the GIF, contract I-523-13.7/97
[5] PPARC Advanced fellow
[6] supported by the Portuguese Foundation for Science and Technology (FCT)
[7] now at Dongshin University, Naju, Korea
[8] now at Northwestern Univ., Evanston/IL, USA
[9] partly supported by the Israel Science Foundation and the Israel Ministry of Science
[10] supported by the Polish State Committee for Scientific Research, grant no. 2 P03B 09322
[11] member of Dept. of Computer Science, supported by the Polish State Committee for Sci. Res., grant no. 2P03B 06116
[12] now at Fermilab, Batavia/IL, USA
[13] on leave from Argonne National Laboratory, USA
[14] now at Max-Planck-Institut für Physik, München/Germany
[15] now at DESY group FEB
[16] on leave of absence at Columbia Univ., Nevis Labs., N.Y./USA
[17] retired
[18] now at Brookhaven National Lab., Upton/NY, USA
[19] now at Mobilcom AG, Rendsburg-Büdelsdorf, Germany
[20] now at Deutsche Börse Systems AG, Frankfurt/Main, Germany
[21] supported by NIKHEF, Amsterdam/NL
[22] also at University of Tokyo
[23] now at LPNHE Ecole Polytechnique, Paris, France
[24] now at Loma Linda University, Loma Linda, CA, USA
[25] now at IBM Global Services, Frankfurt/Main, Germany
[26] now at National Research Council, Ottawa/Canada
[27] on leave of absence at The National Science Foundation, Arlington, VA/USA
[28] present address: Tokyo Metropolitan University of Health Sciences, Tokyo 116-8551, Japan
[29] also at Università del Piemonte Orientale, Novara, Italy
[30] supported by Argonne National Laboratory, USA
[31] also at Łódź University, Poland
[32] supported by the Polish State Committee for Scientific Research, grant no. 2 P03B 07222
[33] supported by the Polish State Committee for Scientific Research, grant no. 2 P03B 00219

[34] Łódź University, Poland
[35] sup. by Pol. State Com. for Scien. Res., 5 P03B 09820 and by Germ. Fed. Min. for Edu. and Research (BMBF), POL 01/043
[36] on leave from MSU, partly supported by University of Wisconsin via the U.S.-Israel BSF

[a] supported by the Natural Sciences and Engineering Research Council of Canada (NSERC)

[b] supported by the German Federal Ministry for Education and Research (BMBF), under contract numbers HZ1GUA 2, HZ1GUB 0, HZ1PDA 5, HZ1VFA 5

[c] supported by the MINERVA Gesellschaft für Forschung GmbH, the Israel Science Foundation, the U.S.-Israel Binational Science Foundation, the Israel Ministry of Science and the Benozyio Center for High Energy Physics

[d] supported by the German-Israeli Foundation, the Israel Science Foundation, and by the Israel Ministry of Science

[e] supported by the Italian National Institute for Nuclear Physics (INFN)

[f] supported by the Japanese Ministry of Education, Science and Culture (the Monbusho) and its grants for Scientific Research

[g] supported by the Korean Ministry of Education and Korea Science and Engineering Foundation

[h] supported by the Netherlands Foundation for Research on Matter (FOM)

[i] supported by the Polish State Committee for Scientific Research, grant no. 620/E-77/SPUB-M/DESY/P-03/DZ 247/2000-2002

[j] partially supported by the German Federal Ministry for Education and Research (BMBF)

[k] supported by the Fund for Fundamental Research of Russian Ministry for Science and Education and by the German Federal Ministry for Education and Research (BMBF)

[l] supported by the Spanish Ministry of Education and Science through funds provided by CICYT

[m] supported by the Particle Physics and Astronomy Research Council, UK

[n] supported by the US Department of Energy

[o] supported by the US National Science Foundation

[p] supported by the Polish State Committee for Scientific Research, grant no. 112/E-356/SPUB-M/DESY/P-03/DZ 301/2000-2002, 2 P03B 13922

[q] supported by the Polish State Committee for Scientific Research, grant no. 115/E-343/SPUB-M/DESY/P-03/DZ 121/2001-2002, 2 P03B 07022

1 Introduction

Deep inelastic scattering (DIS) of leptons on nucleons has been vital in the development of our understanding of the structure of the nucleon. In the Standard Model (SM), charged current (CC) DIS is mediated by the exchange of the W boson. In contrast to neutral current (NC) interactions, where all quark and antiquark flavours contribute, only up-type quarks and down-type antiquarks participate at leading order in e^-p CC DIS reactions. This makes such interactions a powerful tool for flavour-specific investigation of the parton distribution functions (PDFs). Since only left-handed quarks and right-handed antiquarks contribute to CC DIS at HERA, the distribution of the electron-quark centre-of-mass scattering angle, θ^*, is a sensitive probe of the chiral structure of the weak interaction.

Measurements of the CC DIS cross sections at HERA have been reported previously by the H1 [1, 2] and ZEUS [3, 4] collaborations. These data extended the kinematic region covered by fixed-target neutrino-nucleus scattering experiments [5] by about two orders of magnitude in the negative square of the four-momentum transfer, Q^2. In addition, the double-differential e^+p CC DIS cross section, $d^2\sigma/dxdQ^2$, where x is the Bjorken scaling variable, was measured for the first time at high Q^2 by the HERA collider experiments [6, 7]. The mass of the exchanged boson in the space-like domain, extracted from a fit to the differential cross-section $d\sigma/dQ^2$, was consistent with the mass of the W boson measured in time-like processes at LEP and at the Tevatron [8].

This paper presents measurements of the e^-p CC DIS single-differential cross-sections $d\sigma/dQ^2$, $d\sigma/dx$ and $d\sigma/dy$, as well as $d^2\sigma/dxdQ^2$. The results are compared to the expectations of the SM. The measurements are based on 16.4 pb^{-1} of data collected during the running periods in 1998 and 1999 when HERA collided electrons of energy 27.5 GeV with protons of energy 920 GeV, yielding a centre-of-mass energy of 318 GeV. The data represent an increase of a factor of 20 in integrated luminosity over the previous ZEUS e^-p measurement [4]. Cross sections for e^-p CC DIS were reported recently by the H1 collaboration [9].

2 Standard Model prediction

The electroweak Born-level CC DIS differential cross section, $d^2\sigma^{CC}_{\rm Born}/dxdQ^2$, for the reaction $e^-p \to \nu_e X$, with longitudinally unpolarised beams, can be expressed as [10]

$$\frac{d^2\sigma^{CC}_{Born}(e^-p)}{dxdQ^2} = \frac{G_F^2}{4\pi x}\frac{M_W^4}{(Q^2+M_W^2)^2}[Y_+F_2^{CC}(x,Q^2) - y^2F_L^{CC}(x,Q^2) + Y_-xF_3^{CC}(x,Q^2)] \quad (1)$$

where G_F is the Fermi constant, M_W is the mass of the W boson, x is the Bjorken scaling variable, $y = Q^2/xs$ and $Y_\pm = 1 \pm (1-y)^2$. The centre-of-mass energy in the electron-proton collision is given by $\sqrt{s} = 2\sqrt{E_e E_p}$, where E_e and E_p are the electron and proton beam energies, respectively. The inelasticity y is related to θ^* by $y = 1/2(1-\cos\theta^*)$. The structure functions F_2^{CC} and xF_3^{CC}, at leading order in QCD, may be written in terms of sums and differences of quark and antiquark PDFs. For longitudinally unpolarised beams,

$$F_2^{CC} = x[u(x,Q^2) + c(x,Q^2) + \bar{d}(x,Q^2) + \bar{s}(x,Q^2)],$$

$$xF_3^{CC} = x[u(x,Q^2) + c(x,Q^2) - \bar{d}(x,Q^2) - \bar{s}(x,Q^2)],$$

where, for example, the PDF $u(x,Q^2)$ gives the number density of up quarks with momentum fraction x at a given Q^2. The longitudinal structure function, F_L^{CC}, is zero at leading order in QCD. At next-to-leading-order (NLO) in QCD F_L^{CC} is non-zero but gives a negligible contribution to the cross section except at values of y close to 1, where it can be as large as 10%. Since the top-quark mass is large and the off-diagonal elements of the CKM matrix are small [8], the contribution from the third-generation quarks may be ignored in CC DIS at HERA [11]. Since the u-quark density, which is well constrained by NC DIS data, dominates in e^-p CC DIS, the uncertainties coming from the PDFs are small. The uncertainty in the prediction for $d\sigma/dQ^2$, for example, increases from 2% to 5% over the Q^2 range of the present measurements. In the following, uncertainties in the predicted cross sections were obtained using the ZEUS NLO QCD fit [12].

3 The ZEUS experiment

A detailed description of the ZEUS detector can be found elsewhere [13]. A brief outline of the components most relevant for this analysis is given below.

Charged particles are tracked in the central tracking detector (CTD) [14], which operates in a magnetic field of 1.43 T provided by a thin superconducting coil. The CTD consists of 72 cylindrical drift chamber layers, organised in nine superlayers covering the polar-angle[1] region $15^\circ < \theta < 164^\circ$. The relative transverse-momentum resolution for full-length tracks is $\sigma(p_T)/p_T = 0.0058 p_T \oplus 0.0065 \oplus 0.0014/p_T$, with p_T in GeV. The position of the interaction vertex along the beam direction can be reconstructed from the CTD tracks with a resolution of about 1 cm in CC events.

[1] The ZEUS coordinate system is a right-handed Cartesian system, with the Z axis pointing in the proton beam direction, referred to as the "forward direction", and the X axis pointing left towards the centre of HERA. The polar angle, θ, is measured with respect to the proton beam direction. The coordinate origin is at the nominal interaction point.

The high-resolution uranium–scintillator calorimeter (CAL) [15] consists of three parts: the forward (FCAL), the barrel (BCAL) and the rear (RCAL) calorimeters. Each part is subdivided transversely into towers and longitudinally into one electromagnetic section (EMC) and either one (in RCAL) or two (in BCAL and FCAL) hadronic sections (HAC). The smallest subdivision of the calorimeter is called a cell. The CAL relative energy resolutions, as measured under test-beam conditions, are $\sigma(E)/E = 0.18/\sqrt{E}$ for electrons and $\sigma(E)/E = 0.35/\sqrt{E}$ for hadrons (E in GeV). The timing resolution of the CAL is better than 1 ns for energy deposits greater than 4.5 GeV. The position of the interaction vertex along the beam direction can be reconstructed from the arrival time of energy deposits in FCAL. The resolution is about 9 cm for events with FCAL energy above 25 GeV, improving to about 7 cm for FCAL energy above 100 GeV.

An instrumented-iron backing calorimeter (BAC) [16] surrounds the CAL and can be used to measure energy leakage and identify muons. Muon chambers in the forward, barrel and rear [17] regions are used in this analysis to veto background events induced by cosmic-ray or beam-halo muons.

The luminosity was measured using the Bethe-Heitler reaction $ep \to e\gamma p$. The photons were measured by the luminosity monitor [18], a lead-scintillator calorimeter placed in the HERA tunnel 107 m from the interaction point in the electron beam direction.

4 Monte Carlo simulation

Monte Carlo (MC) simulation was used to determine the efficiency for selecting events and the accuracy of kinematic reconstruction, to estimate the ep background rates and to extract cross sections for the full kinematic region. A sufficient number of events was generated to ensure that the statistical uncertainties arising from the MC simulation were negligible compared to those of the data. The MC samples were normalised to the total integrated luminosity of the data.

The ZEUS detector response was simulated with a program based on GEANT 3.13 [19]. The generated events were passed through the simulated detector, subjected to the same trigger requirements as the data, and processed by the same reconstruction programs.

Charged current DIS events, including electroweak radiative effects, were simulated using the HERACLES 4.6.1 [20] program with the DJANGOH 1.1 [21] interface to the MC generators that provide the hadronisation. Corrections for initial-state radiation, vertex and propagator corrections and two-boson exchange are included in HERACLES. The mass of the W boson was calculated using the PDG [8] values for the fine structure constant,

the Fermi constant, the mass of the Z boson and the mass of the top quark, and with the Higgs-boson mass set to 100 GeV. The colour-dipole model of ARIADNE 4.10 [22] was used to simulate the $\mathcal{O}(\alpha_S)$ plus leading logarithmic corrections to the result of the quark-parton model. As a systematic check, the MEPS model of LEPTO 6.5 [23] was used. Both programs use the Lund string model of JETSET 7.4 [24] for the hadronisation. A set of NC events generated with DJANGOH was used to estimate the NC contamination in the CC sample. Photoproduction background was estimated using events simulated with HERWIG 5.9 [25]. The background from W production was estimated using the EPVEC [26] generator, and the background from production of charged-lepton pairs was generated with the LPAIR [27] program.

5 Reconstruction of kinematic variables

The principal signature of CC DIS at HERA is the presence of a large missing transverse momentum, $P_{T,\mathrm{miss}}$, arising from the energetic final-state neutrino that escapes detection. The quantity $P_{T,\mathrm{miss}}$ was calculated from

$$P^2_{T,\mathrm{miss}} = P^2_X + P^2_Y = \left(\sum_i E_i \sin\theta_i \cos\phi_i\right)^2 + \left(\sum_i E_i \sin\theta_i \sin\phi_i\right)^2 ,$$

where the sums run over all calorimeter energy deposits, E_i (uncorrected in the trigger, but corrected in the offline analysis for energy loss in inactive material etc. [28]) and θ_i and ϕ_i are the polar and azimuthal angles of the calorimeter deposits as viewed from the interaction vertex. The polar angle of the hadronic system, γ_h, is defined by $\cos\gamma_h = (P^2_{T,\mathrm{miss}} - \delta^2)/(P^2_{T,\mathrm{miss}} + \delta^2)$, where $\delta = \sum(E_i - E_i\cos\theta_i) = \sum(E - P_z)_i$. In the naive quark-parton model, γ_h is the angle through which the struck quark is scattered. Finally, the total transverse energy, E_T, is given by $E_T = \sum E_i \sin\theta_i$.

The kinematic variables were reconstructed using the Jacquet-Blondel method [29]. The estimators of y, Q^2 and x are: $y_{JB} = \delta/(2E_e)$, $Q^2_{JB} = P^2_{T,\mathrm{miss}}/(1 - y_{JB})$, and $x_{JB} = Q^2_{JB}/(s y_{JB})$.

6 Event selection

Charged current DIS candidates were selected by requiring a large $P_{T,\mathrm{miss}}$ and a reconstructed event vertex consistent with an ep interaction. The main sources of background come from NC scattering and high-E_T photoproduction. The energy resolution of the

CAL or the energy that escapes detection can lead to significant missing transverse momentum. Events not from ep collisions, such as beam-gas interactions, beam-halo muons or cosmic rays can also cause substantial apparent imbalance in the transverse momentum and so constitute other sources of background. The selection criteria described below were imposed to separate CC events from all backgrounds.

When the current jet lies in the central region of the detector, i.e. γ_h is large, tracks in the CTD can be used to reconstruct an event vertex, strongly suppressing non-ep backgrounds. The procedure designed to select these events is described in Section 6.2. For CC events with small γ_h, the charged particles from the hadronic final state are often outside the acceptance of the CTD. Such events populate the high-x region of the kinematic plane. The algorithm designed specifically to select such events is described in Section 6.3. The events were classified first according to γ_0, the value of γ_h measured with respect to the nominal interaction point. Subsequently, the kinematic quantities were recalculated using the Z-coordinate of the event vertex ($Z_{\rm VTX}$) determined from either CTD tracks or the calorimeter-timing information discussed in Section 3.

In the data-taking period, the HERA proton beam contained a significant number of off-axis protons. Such particles passed through the ZEUS interaction region displaced horizontally by several millimeters from the nominal trajectory and gave rise to an especially pernicious class of off-axis beam-gas interactions. In order to remove this background, several selection requirements had to be made more restrictive than was the case in the previous ZEUS study [6].

6.1 Trigger selection

ZEUS has a three-level trigger system [13]. At the first level, events were selected using criteria based on the energy, transverse energy and missing transverse momentum measured in the calorimeter. Generally, events were triggered with a low threshold on these quantities when a coincidence with CTD tracks from the event vertex was required, while a higher threshold was necessary for events with no CTD tracks. The latter class of events has a hadronic final state boosted forward outside the CTD acceptance. Typical threshold values were 5 GeV (8 GeV) in missing transverse momentum, or 11.5 GeV (21 GeV) in transverse energy for events with (without) CTD tracks.

At the second level, timing information from the calorimeter was used to reject events inconsistent with the bunch-crossing time. In addition, the topology of the CAL energy deposits was used to reject background events. In particular, since the resolution of the missing transverse momentum is better at the second level than at the first level, a tighter cut of 6 GeV (9 GeV for events without CTD tracks) was made.

At the third level, track reconstruction and vertex finding were performed and used to reject candidate events with a vertex inconsistent with the beam interaction envelope. Cuts were applied to calorimeter quantities and reconstructed tracks to reduce beam-gas contamination further.

6.2 Offline selection based on a CTD vertex

Events with $\gamma_0 > 0.4$ rad were required to have a vertex reconstructed from CTD tracks and to satisfy all of the following criteria:

- $|Z_{\rm VTX}| < 50$ cm
  the primary vertex reconstructed from the CTD tracks was required to be within the range consistent with the *ep* interaction region;
- $P_{T,\rm miss} > 12$ GeV and $P'_{T,\rm miss} > 10$ GeV
  $P'_{T,\rm miss}$ is the missing transverse momentum calculated excluding the FCAL towers closest to the beam hole. The $P'_{T,\rm miss}$ cut strongly suppresses beam-gas events while maintaining high efficiency for CC events;
- Tracking requirement
  at least one track associated with the event vertex must have transverse momentum in excess of 0.2 GeV and a polar angle in the range 15° to 164°. In order to remove off-axis beam-gas background, a cut was also applied in two dimensions on the number of such "good" tracks, $N_{\rm good}$, versus the total number of tracks, $N_{\rm trks}$ [30];
- Rejection of photoproduction
  $P_{T,\rm miss}/E_T > 0.5$ was required for events with $P_{T,\rm miss} < 30$ GeV. This cut selected a collimated energy flow, as expected from a single scattered quark. No $P_{T,\rm miss}/E_T$ requirement was imposed on the events with $P_{T,\rm miss} \geq 30$ GeV. In addition, the difference between the direction of the (P_X, P_Y) vector calculated using CTD tracks and that obtained using the CAL was required to be less than 0.5 radians for $P_{T,\rm miss} < 30$ GeV and less than 2.0 radians for $P_{T,\rm miss} \geq 30$ GeV;
- Rejection of NC DIS
  NC DIS events in which the scattered electron or jet energy was poorly measured could have a large apparent missing transverse momentum. To identify such events, a search for candidate electrons was made using an electron-finding algorithm that selects isolated electromagnetic clusters in the CAL [31]. Candidate electron clusters within the CTD acceptance were required to have an energy above 4 GeV and a matching track with momentum larger than 25% of the cluster energy. Clusters with $\theta > 164°$ were required to have a transverse momentum exceeding 2 GeV. Events with a candidate electron satisfying the above criteria and $\delta > 20$ GeV were rejected. For

contained NC events, δ peaks at $2E_e = 55\,\text{GeV}$. This cut was only applied for events with $P_{T,\text{miss}} < 30\,\text{GeV}$;

- Rejection of non-ep background
  beam-gas events typically gave CAL times that were inconsistent with the bunch-crossing time. Such events were rejected. Muon-finding algorithms based on CAL energy deposits or muon-chamber signals were used to reject events produced by cosmic rays or muons in the beam halo.

6.3 Offline selection based on a CAL vertex

For events with $\gamma_0 < 0.4$ rad, the following criteria were imposed:

- $|Z_{\text{VTX}}| < 50$ cm
  Z_{VTX} was reconstructed from the measured arrival time of energy deposits in FCAL [32];
- $P_{T,\text{miss}} > 25\,\text{GeV}$ and $P'_{T,\text{miss}} > 25\,\text{GeV}$
  to remove off-axis beam-gas events, the conditions on missing transverse momentum were tightened, compensating for the relaxation of the requirements on tracks;
- Rejection of non-ep background
  the timing and muon-rejection cuts described in Section 6.2 were used. A class of background events that were especially troublesome in this selection branch arose from beam-halo muons that produced a shower inside the FCAL. To reduce this background, topological cuts on the transverse and longitudinal shower shape were imposed; these cuts rejected events in which the energy deposits were much more strongly collimated than for typical hadronic jets.

6.4 Final event sample

To restrict the sample to regions where the resolution in the kinematic variables was good and the backgrounds small, the requirements $Q^2_{JB} > 200\,\text{GeV}^2$ and $y_{JB} < 0.9$ were imposed. All events were visually inspected, and nine cosmic-ray and halo-muon events were removed. The final $e^- p$ sample consisted of 650 events, to be compared with 660 predicted by the MC simulation.

The resolution in Q^2 is $\sim 25\%$ over the entire Q^2 range. The resolution in x improves from $\sim 25\%$ at $x = 0.01$ to $\sim 10\%$ at $x = 0.5$. The resolution in y is $\sim 13\%$ over the entire range.

Figure 1 compares the distributions of data events entering the final CC sample with the MC expectation for the sum of the CC signal and ep background events. The MC simulation gives a good description of the data.

7 Cross-section determination and systematic uncertainties

7.1 Cross-section determination

Monte Carlo events were generated according to Eq. (1), including electroweak radiative effects. The value of the cross section, at a fixed point within a bin, was obtained from the ratio of the number of observed events, from which the estimated background had been subtracted, to the number of events predicted by the MC simulation, multiplied by the cross section obtained using Eq. (1). Consequently, the acceptance, bin-centring and radiative corrections were all taken from the MC simulation.

7.2 Systematic uncertainties

The major sources of systematic uncertainty in the cross sections are discussed below:

- Uncertainty of the calorimeter energy scale
  the hadronic energy scale and the associated uncertainty were determined, using NC DIS events, from the ratios of the total hadronic transverse momentum, $P_{T,\mathrm{had}}$, to $P_{T,\mathrm{DA}}$ and $P_{T,\mathrm{e}}$, where $P_{T,\mathrm{DA}} = \sqrt{Q^2_{\mathrm{DA}}\,(1-y_{\mathrm{DA}})}$ is the transverse momentum obtained from the double-angle method [33] and $P_{T,\mathrm{e}}$ is the measured transverse momentum of the scattered electron. In order to restrict the hadronic activity to particular polar-angle regions, a sample of NC DIS events with a single hadronic jet was selected. By applying suitable cuts on the location of the current jet and evaluating $P_{T,\mathrm{had}}/P_{T,\mathrm{DA}}$ and $P_{T,\mathrm{had}}/P_{T,\mathrm{e}}$ event by event, the hadronic energy scales of the FCAL and BCAL were determined. The responses of the HAC and EMC sections of the individual calorimeters were determined by plotting $P_{T,\mathrm{had}}/P_{T,\mathrm{DA}}$ and $P_{T,\mathrm{had}}/P_{T,\mathrm{e}}$ as a function of the fraction of the hadronic energy measured in the EMC section of the calorimeter. In each case, the uncertainty was found by comparing the determinations from data and MC. In order to study the hadronic energy scale in the RCAL, a sample of diffractive DIS events was selected. Such events are characterised by a large gap in the hadronic energy flow between the proton remnant and the current jet. $P_{T,\mathrm{had}}/P_{T,\mathrm{DA}}$ was evaluated event-by-event for events with hadronic activity exclusively in the RCAL and the energy scale and associated uncertainty determined.

  The relative uncertainty in the hadronic energy scale was determined to be 2% for the RCAL and 1% for the FCAL and BCAL. Varying the energy scale of the calorimeter sections by these amounts in the detector simulation induces small shifts of the Jacquet-Blondel estimators for the kinematic variables. Varying the energy scale of

each of the calorimeters simultaneously up or down by these amounts in the detector simulation gives one estimate of the systematic uncertainty. A second estimate was obtained by increasing (decreasing) the FCAL and RCAL energy scales together while the BCAL energy scale was decreased (increased). A third estimate was made by simultaneously increasing the energy measured in the EMC section of the calorimeter by 2% and decreasing the energy measured in the HAC section by 2% and vice-versa. This was done separately for each of the calorimeters. The final systematic error attributed to the uncertainty in the hadronic energy scale was obtained by taking the quadratic sum of these three estimates. The resulting systematic shifts in the measured cross sections were typically within $\pm 5\%$, but increase to $+10\%$ in the highest y bin and $\pm(10-20)\%$ in the highest Q^2 and x bins;

- Energy leakage
  four percent of the accepted events have a measurable energy leakage from the CAL into the BAC. The average transverse-energy leakage for these events is 5% of the E_T observed in the CAL. Both the fraction of events with leakage and the average leakage are well modelled by the MC simulation and the effect on the cross-section measurement is negligible;

- Variation of selection thresholds
  for the majority of the kinematic bins, varying the selection thresholds by $\pm 10\%$ in both data and MC resulted in small changes in the measured cross sections. However, varying the $P_{T,\mathrm{miss}}/E_T$ threshold gave a change in the cross section of around $\pm 10\%$ at low Q^2 in $d\sigma/dQ^2$ and up to $\pm(10-20)\%$ in the bins of the double-differential cross section. Varying the $P'_{T,\mathrm{miss}}$ cut gave a change of approximately $+10\%$ in the single-differential cross-section $d\sigma/dy$ at the lowest y. Varying the $P_{T,\mathrm{miss}}$ cut gave a change of -12% in the lowest-Q^2 bin of $d\sigma/dQ^2$. The tracking requirement for $P_{T,\mathrm{miss}} < 30$ GeV was tightened and gave changes in the cross section of $+8\%$ and -12% in the lowest-Q^2 bins of $d\sigma/dQ^2$ and -10% in the highest y bin of $d\sigma/dy$. Changes of $\pm(10-20)\%$ were observed in the lowest-Q^2 bins of the double-differential cross section;

- Uncertainty in the parton-shower scheme
  the MEPS model of LEPTO was used to calculate the acceptance instead of the ARIADNE model. The largest effects were observed in the bins of low Q^2 ($\pm 8\%$), highest and lowest y ($\pm 5\%$) and low x ($\pm 4\%$). The largest effect in the double-differential cross section was seen in the low-Q^2 and low-x bins, where it amounted to $\pm(10-13)\%$;

- Background subtraction
  the uncertainty in the photoproduction background was estimated by fitting a linear combination of the $P_{T,\mathrm{miss}}/E_T$ distributions of the signal and the background MC samples to the corresponding distribution in the data, allowing the normalisation

(N_{PhP}) of the photoproduction MC events to vary. No cut on $P_{T,\mathrm{miss}}/E_T$ was applied for this check. N_{PhP} was varied in the range $N_{PhP}/2$ to $2{\cdot}N_{PhP}$. This range corresponds to the uncertainty given by the fit and changes in the cross sections were found to be within $\pm 1\%$;

- Trigger efficiency
  the simulation of the efficiency of the first-level trigger as a function of $P_{T,\mathrm{miss}}$ was examined by using data events triggered by an independent trigger branch that was highly efficient for CC events, since it was based on CAL energy sums. The difference between the efficiencies calculated from the data and from MC events had a negligible effect on the measured cross section;

- Choice of parton distribution functions
  the CC MC events were generated using the CTEQ5D PDFs [34]. The ZEUS NLO QCD fit [12] was used to examine the influence of variations of the PDFs on the cross-section measurement. Monte Carlo events were re-weighted to reflect the uncertainty from the fit and new acceptance-correction factors were computed. The change in the measured cross section was typically $< 1\%$, except at low Q^2 where it was -2% and at high x where it was $+3\%$;

- The effect of F_L
  the DJANGOH program neglects the F_L contribution to $d^2\sigma/dxdQ^2$ when generating CC events. The corresponding effect on the acceptance-correction factors was evaluated by re-weighting MC events with the ratio of the cross sections with and without F_L. The largest effect was observed in the highest-y bin where it was -2%;

- Uncertainty in the radiative correction
  the magnitude of the $\mathcal{O}(\alpha)$ electroweak corrections to CC DIS have been discussed by several authors [35, 36]. Various theoretical approximations and computer codes gave differences in the CC cross sections of typically $\leq \pm(1-2)\%$. The differences can be as large as $\pm(3-8)\%$ at high x and at high y. This uncertainty was not included in the total systematic uncertainty.

The individual uncertainties were added in quadrature separately for the positive and negative deviations from the nominal cross-section values to obtain the total systematic uncertainty listed in Tables 1 and 2. The uncertainty on the luminosity of 1.8% was not included.

8 Results

The single-differential cross-sections $d\sigma/dQ^2$, $d\sigma/dx$ and $d\sigma/dy$ for $Q^2 > 200$ GeV^2 are shown in Fig. 2 and compiled[2] in Table 1. The cross sections $d\sigma/dQ^2$ and $d\sigma/dx$ were extrapolated to the full y range using the SM predictions with CTEQ5D PDFs. The SM cross sections derived from Eq. (1) using the ZEUS NLO QCD fit, CTEQ5D [34] and MRST(99) [37] parameterisations of the PDFs are also shown, together with the ratios of the measured cross sections to the SM cross section evaluated with the ZEUS NLO QCD fit. The Standard Model gives a good description of the data.

The reduced double-differential cross section, $\tilde{\sigma}$, is defined by

$$\tilde{\sigma} = \left[\frac{G_F^2}{2\pi x}\left(\frac{M_W^2}{M_W^2+Q^2}\right)^2\right]^{-1} \frac{d^2\sigma}{dx\,dQ^2}.$$

At leading order in QCD, $\tilde{\sigma}(e^-p \to \nu_e X)$ depends on the quark momentum distributions as follows:

$$\tilde{\sigma}(e^-p \to \nu_e X) = x\left[u + c + (1-y)^2(\bar{d}+\bar{s})\right]. \tag{2}$$

The reduced cross sections are displayed versus Q^2 and x in Figs. 3 and 4, respectively, and compiled[2] in Table 2. The predictions of Eq. (1), evaluated using the ZEUS NLO QCD fit, give a good description of the data. The PDF combinations $(u+c)$ and $(\bar{d}+\bar{s})$, obtained in the $\overline{\rm MS}$ scheme from the ZEUS NLO QCD fit, are shown separately in Fig. 4.

The W boson couples only to left-handed fermions and right-handed antifermions. Thus, in the quark-parton-model description of e^-p CC DIS, the Z component of the total angular momentum of the initial-state electron-quark system is zero for e^-q scattering and one unit of angular momentum for $e^-\bar{q}$ scattering. Therefore, the angular distribution of the scattered quark in e^-q CC DIS will be flat, while it will exhibit a $(1+\cos\theta^*)^2$ distribution in $e^-\bar{q}$ scattering. Since $(1-y)^2 = 1/4(1+\cos\theta^*)^2$ the helicity structure of CC interactions can be illustrated by plotting the reduced double-differential cross section of Eq. (2) versus $(1-y)^2$ in bins of fixed x. At leading order in QCD, in the region of approximate scaling, this yields a straight line, the intercept of which gives the $(u+c)$ contribution, while the slope gives the $(\bar{d}+\bar{s})$ contribution.

Figure 5 shows the e^-p CC DIS data, compared to the previously published e^+p data [6]. At large x, e^-p CC DIS is sensitive to the u-valence-quark PDF while e^+p CC DIS is sensitive to the d-valence-quark PDF. At leading order in QCD, the reduced double-differential cross section for e^+p CC DIS can be written as

$$\tilde{\sigma}(e^+p \to \bar{\nu}_e X) = x\left[\bar{u} + \bar{c} + (1-y)^2(d+s)\right],$$

[2] Tables 3 and 4 contain details of the systematic uncertainties that are correlated between cross-section bins.

permitting a similar interpretation for the intercept and slope in terms of the appropriate parton densities. Scaling violations can be observed in the theoretical prediction as $(1-y)^2$ approaches 1. The data agree with the expectation of the SM from the ZEUS NLO QCD fit, which is also shown.

The total cross section for e^-p CC DIS in the kinematic region $Q^2 > 200\,\mathrm{GeV}^2$ is

$$\sigma^{\mathrm{CC}}_{\mathrm{TOT}}(Q^2 > 200\ \mathrm{GeV}^2) = 66.7 \pm 2.7(\mathrm{stat.})^{+1.8}_{-1.1}(\mathrm{syst.})\ \mathrm{pb}.$$

The result is in good agreement with the SM expectation, evaluated using the ZEUS NLO QCD fit, of $69.0^{+1.6}_{-1.3}$ pb.

9 Electroweak analysis

Equation (1) shows that the magnitude of the CC DIS cross section is determined by G_F and the PDFs. The fall in the cross section with increasing Q^2 is dominated by the propagator term, $M_W^4/(Q^2+M_W^2)^2$. Figure 3 shows that the Q^2 dependence of the PDFs is small by comparison. An electroweak analysis, performed by fitting $d\sigma/dQ^2$ with G_F fixed at the PDG [8] value of $1.16639 \cdot 10^{-5}\,\mathrm{GeV}^{-2}$ and M_W treated as a free parameter gives

$$M_W = 80.3 \pm 2.1\,(\mathrm{stat.}) \pm 1.2\,(\mathrm{syst.}) \pm 1.0\,(\mathrm{PDF})\ \mathrm{GeV},$$

where the third uncertainty was estimated by varying the PDFs within the uncertainties given by the ZEUS NLO QCD fit [12]. The systematic uncertainty includes contributions from the sources identified in Section 7.2 and the uncertainty on the measured luminosity. This measurement, in the space-like region, is in good agreement with the more precise measurements of W-boson production in the time-like region [8]. This measurement is also in good agreement with the previous ZEUS measurement of $M_W = 81.4^{+2.7}_{-2.6}(\mathrm{stat.}) \pm 2.0(\mathrm{syst.})^{+3.3}_{-3.0}(\mathrm{PDF})\,\mathrm{GeV}$ obtained by a fit to $d\sigma/dQ^2$ for e^+p CC DIS at $\sqrt{s} = 300$ GeV [6]. The present measurement has a smaller statistical uncertainty than the previous result, despite a lower integrated luminosity, due to the larger cross section for CC DIS in e^-p scattering compared to e^+p scattering. The measurement also benefits from improved understanding of the detector, leading to a smaller systematic uncertainty. Since the u-quark density, which is well constrained by NC DIS data, dominates in e^-p CC DIS, the uncertainty coming from the PDFs is smaller than in the case of e^+p CC DIS, where the d-quark density dominates.

10 Summary

Differential cross sections for charged current deep inelastic scattering, $e^- p \to \nu_e X$, have been measured for $Q^2 > 200$ GeV^2 using 16.4 pb^{-1} of data collected with the ZEUS detector during the period 1998 to 1999. The double-differential cross-section $d^2\sigma/dx\,dQ^2$ has been measured in the kinematic range $280\,\text{GeV}^2 < Q^2 < 30\,000\,\text{GeV}^2$ and $0.015 < x < 0.42$. The chiral structure of the Standard Model was investigated by plotting the double-differential cross section as a function of $(1-y)^2$. The Standard Model gives a good description of the data. The mass of the W boson has been determined, from the Q^2 dependence of the measured cross section, to be $M_W = 80.3 \pm 2.1\,(\text{stat.}) \pm 1.2\,(\text{syst.}) \pm 1.0\,(\text{PDF})$ GeV.

Acknowledgements

We appreciate the contributions to the construction and maintenance of the ZEUS detector of the many people who are not listed as authors. The HERA machine group and the DESY computing staff are especially acknowledged for their success in providing excellent operation of the collider and the data-analysis environment. We thank the DESY directorate for their strong support and encouragement.

References

[1] H1 Collaboration, T. Ahmed et al., Phys. Lett. B 324 (1994) 241;
H1 Collaboration, S. Aid et al., Z. Phys. C 67 (1995) 565.

[2] H1 Collaboration, S. Aid et al., Phys. Lett. B 379 (1996) 319.

[3] ZEUS Collaboration, M. Derrick et al., Phys. Rev. Lett. 75 (1995) 1006.

[4] ZEUS Collaboration, M. Derrick et al., Z. Phys. C 72 (1996) 47.

[5] CDHS Collaboration, H. Abramowicz et al., Z. Phys. C 25 (1984) 29;
CDHSW Collaboration, J.P. Berge et al., Z. Phys. C 49 (1991) 187;
CCFR Collaboration, E. Oltman et al., Z. Phys. C 53 (1992) 51;
BEBC Collaboration, G.T. Jones et al., Z. Phys. C 62 (1994) 575.

[6] ZEUS Collaboration, J. Breitweg et al., Eur. Phys. J. C 12 (2000) 411.

[7] H1 Collaboration, C. Adloff et al., Eur. Phys. J. C 13 (2000) 609.

[8] Particle Data Group, D.E. Groom et al., Eur. Phys. J. C 15 (2000) 1.

[9] H1 Collaboration, C. Adloff et al., Eur. Phys. J. C 19 (2001) 269.

[10] A.M. Cooper-Sarkar, R.C.E. Devenish and A. De Roeck, Int. J. Mod. Phys.
A 13 (1998) 3385.

[11] U.F. Katz, *Deep-Inelastic Positron–Proton Scattering in the High-Momentum-Transfer Regime of HERA*, Springer Tracts in Modern Physics, Vol. 168. Springer, Berlin, Heidelberg, 2000.

[12] ZEUS Collaboration, S. Chekanov et al., Eur. Phys. J. C 21 (2001) 443.

[13] ZEUS Collaboration, U. Holm (ed.), *The ZEUS Detector*. Status Report (unpublished), DESY (1993), available on `http://www-zeus.desy.de/bluebook/bluebook.html`.

[14] N. Harnew et al., Nucl. Inst. Meth. A 279 (1989) 290;
B. Foster et al., Nucl. Phys. Proc. Suppl. B 32 (1993) 181;
B. Foster et al., Nucl. Inst. Meth. A 338 (1994) 254.

[15] M. Derrick et al., Nucl. Inst. Meth. A 309 (1991) 77;
A. Andresen et al., Nucl. Inst. Meth. A 309 (1991) 101;
A. Caldwell et al., Nucl. Inst. Meth. A 321 (1992) 356;
A. Bernstein et al., Nucl. Inst. Meth. A 336 (1993) 23.

[16] H. Abramowicz et al., Nucl. Inst. Meth. A 313 (1992) 126.

[17] G. Abbiendi et al., Nucl. Inst. Meth. A 333 (1993) 342.

[18] J. Andruszków et al., Preprint DESY-92-066, DESY, 1992;
ZEUS Collaboration, M. Derrick et al., Z. Phys. C 63 (1994) 391;
J. Andruszków et al., Acta Phys. Pol. B 32 (2001) 2025.

[19] R. Brun et al., GEANT3, Technical Report CERN-DD/EE/84-1, CERN, 1987.

[20] A. Kwiatkowski, H. Spiesberger and H.-J. Möhring, Comp. Phys. Comm. 69 (1992) 155. Also in *Proc. Workshop Physics at HERA*, 1991, DESY, Hamburg;
H. Spiesberger, *An Event Generator for ep Interactions at HERA Including Radiative Processes (Version 4.6)*, 1996, available on `http://www.desy.de/~hspiesb/heracles.html`.

[21] H. Spiesberger, HERACLES *and* DJANGOH*: Event Generation for ep Interactions at HERA Including Radiative Processes*, 1998, available on `http://www.desy.de/~hspiesb/djangoh.html`.

[22] L. Lönnblad, Comp. Phys. Comm. 71 (1992) 15.

[23] G. Ingelman, A. Edin and J. Rathsman, Comp. Phys. Comm. 101 (1997) 108.

[24] T. Sjöstrand, Comp. Phys. Comm. 39 (1986) 347;
T. Sjöstrand and M. Bengtsson, Comp. Phys. Comm. 43 (1987) 367;
T. Sjöstrand, Comp. Phys. Comm. 82 (1994) 74.

[25] G. Marchesini et al., Comp. Phys. Comm. 67 (1992) 465.

[26] U. Baur, J.A.M. Vermaseren and D. Zeppenfeld, Nucl. Phys. B 375 (1992) 3.

[27] S.P. Baranov et al., *Proc. Workshop on Physics at HERA*, W. Buchmüller and G. Ingelman (eds.), Vol. 3, p. 1478. DESY, Hamburg, Germany (1991).

[28] ZEUS Collaboration, J. Breitweg et al., Eur. Phys. J. C 11 (1999) 427.

[29] F. Jacquet and A. Blondel, *Proceedings of the Study for an ep Facility for Europe*, U. Amaldi (ed.), p. 391. Hamburg, Germany (1979). Also in preprint DESY 79/48.

[30] A.D. Tapper, *Measurement of charged current deep inelastic scattering cross sections using the ZEUS detector at HERA*. Ph.D. Thesis, University of London, 2001. (unpublished).

[31] H. Abramowicz, A. Caldwell and R. Sinkus, Nucl. Inst. Meth. A 365 (1995) 508.

[32] ZEUS Collaboration, M. Derrick et al., Phys. Lett. B 316 (1993) 412.

[33] S. Bentvelsen, J. Engelen and P. Kooijman, *Proc. Workshop on Physics at HERA*, W. Buchmüller and G. Ingelman (eds.), Vol. 1, p. 23. Hamburg, Germany, DESY (1992);
K.C. Höger, *Proc. Workshop on Physics at HERA*, W. Buchmüller and G. Ingelman (eds.), Vol. 1, p. 43. Hamburg, Germany, DESY (1992).

[34] CTEQ Collaboration, H.L. Lai et al., Eur. Phys. J. C 12 (2000) 375.

[35] A.M. Cooper-Sarkar et al., J. Phys. G 25 (1999) 1387.

[36] B. Heinemann, S. Riess and H. Spiesberger, *Proc. Workshop on Monte Carlo Generators for HERA Physics*, G. Grindhammer et al. (ed.), p. 530. DESY, Hamburg, Germany (1999). Also in preprint DESY-PROC-1999-02, available on `http://www.desy.de/~heramc/`.

[37] A.D. Martin et al., Nucl. Phys. Proc. Suppl. B 79 (1999) 105. *contrib. to* 7^{th} *Int. Workshop on Deep Inelastic Scattering and QCD (DIS99),* J. Blümlein and T. Riemann (eds.). Zeuthen, Germany, April 1999.

$d\sigma/dQ^2$				
Q^2 range (GeV^2)	Q^2 (GeV^2)	$\mathrm{N_{DATA}}$	$\mathrm{N_{BG}}$	$d\sigma/dQ^2$ (pb/ GeV^2)
200 - 400	280	18	1.0	$(2.51 \pm 0.63^{+0.53}_{-0.46}) \cdot 10^{-2}$
400 - 711	530	33	0.3	$(2.70 \pm 0.48^{+0.35}_{-0.44}) \cdot 10^{-2}$
711 - 1265	950	83	1.1	$(2.13 \pm 0.24^{+0.13}_{-0.13}) \cdot 10^{-2}$
1265 - 2249	1700	134	0.8	$(1.22 \pm 0.11^{+0.04}_{-0.04}) \cdot 10^{-2}$
2249 - 4000	3000	138	0.7	$(6.32 \pm 0.55^{+0.13}_{-0.17}) \cdot 10^{-3}$
4000 - 7113	5300	117	0.5	$(2.88 \pm 0.27^{+0.10}_{-0.11}) \cdot 10^{-3}$
7113 - 12649	9500	90	0.3	$(1.24 \pm 0.13^{+0.04}_{-0.05}) \cdot 10^{-3}$
12649 - 22494	17000	30	0.2	$(2.37 \pm 0.44^{+0.16}_{-0.13}) \cdot 10^{-4}$
22494 - 60000	30000	7	0.1	$(2.68^{+1.46\ +0.30}_{-1.00\ -0.36}) \cdot 10^{-5}$
$d\sigma/dx$				
x range	x	$\mathrm{N_{DATA}}$	$\mathrm{N_{BG}}$	$d\sigma/dx$ (pb)
0.010 - 0.021	0.015	35	1.0	$(6.08 \pm 1.08^{+0.61}_{-0.56}) \cdot 10^{2}$
0.021 - 0.046	0.032	81	0.9	$(4.23 \pm 0.48^{+0.22}_{-0.33}) \cdot 10^{2}$
0.046 - 0.100	0.068	172	1.5	$(2.76 \pm 0.22^{+0.05}_{-0.07}) \cdot 10^{2}$
0.100 - 0.178	0.130	168	0.7	$(1.87 \pm 0.15^{+0.04}_{-0.03}) \cdot 10^{2}$
0.178 - 0.316	0.240	128	0.2	$(8.08 \pm 0.72^{+0.19}_{-0.17}) \cdot 10^{1}$
0.316 - 0.562	0.420	55	0.1	$(2.48 \pm 0.34^{+0.15}_{-0.10}) \cdot 10^{1}$
0.562 - 1.000	0.650	2	0.1	$(1.28^{+1.75\ +0.19}_{-0.86\ -0.16}) \cdot 10^{0}$
$d\sigma/dy$				
y range	y	$\mathrm{N_{DATA}}$	$\mathrm{N_{BG}}$	$d\sigma/dy$ (pb)
0.00 - 0.10	0.05	67	0.6	$(1.40 \pm 0.17^{+0.12}_{-0.03}) \cdot 10^{2}$
0.10 - 0.20	0.15	146	0.8	$(1.18 \pm 0.10^{+0.05}_{-0.05}) \cdot 10^{2}$
0.20 - 0.34	0.27	153	0.6	$(8.85 \pm 0.73^{+0.26}_{-0.43}) \cdot 10^{1}$
0.34 - 0.48	0.41	95	0.7	$(5.63 \pm 0.59^{+0.20}_{-0.16}) \cdot 10^{1}$
0.48 - 0.62	0.55	86	0.9	$(5.40 \pm 0.59^{+0.18}_{-0.19}) \cdot 10^{1}$
0.62 - 0.76	0.69	70	0.4	$(5.07 \pm 0.62^{+0.19}_{-0.30}) \cdot 10^{1}$
0.76 - 0.90	0.83	33	1.0	$(3.01 \pm 0.55^{+0.35}_{-0.30}) \cdot 10^{1}$

Table 1: *Values of the differential cross-sections $d\sigma/dQ^2$, $d\sigma/dx$ and $d\sigma/dy$. The following quantities are given: the range of the measurement; the value at which the cross section is quoted; the number of data events, N_{DATA}; the number of expected background events, N_{BG} and the measured cross section, with statistical and systematic uncertainties.*

Q^2 (GeV^2)	x	$\mathrm{N_{DATA}}$	$\mathrm{N_{BG}}$	$\tilde{\sigma}$
280	0.032	7	0.3	$0.64^{+0.36\ +0.13}_{-0.25\ -0.06}$
530	0.015	10	0.0	$1.13^{+0.49\ +0.14}_{-0.36\ -0.26}$
530	0.032	12	0.1	$0.91^{+0.35\ +0.08}_{-0.26\ -0.16}$
530	0.068	8	0.0	$0.83^{+0.41\ +0.14}_{-0.29\ -0.19}$
950	0.015	17	0.7	$1.51 \pm 0.39^{+0.25}_{-0.28}$
950	0.032	16	0.1	$0.75 \pm 0.19^{+0.08}_{-0.08}$
950	0.068	29	0.2	$1.01 \pm 0.19^{+0.13}_{-0.13}$
950	0.130	17	0.1	$0.79 \pm 0.19^{+0.11}_{-0.09}$
1700	0.032	31	0.2	$0.87 \pm 0.16^{+0.11}_{-0.05}$
1700	0.068	51	0.3	$0.81 \pm 0.12^{+0.02}_{-0.05}$
1700	0.130	32	0.1	$0.75 \pm 0.13^{+0.03}_{-0.05}$
1700	0.240	18	0.0	$0.47 \pm 0.11^{+0.01}_{-0.02}$
3000	0.068	56	0.5	$0.71 \pm 0.10^{+0.04}_{-0.01}$
3000	0.130	34	0.1	$0.58 \pm 0.10^{+0.03}_{-0.02}$
3000	0.240	27	0.0	$0.49 \pm 0.09^{+0.01}_{-0.01}$
3000	0.420	8	0.0	$0.21^{+0.10\ +0.02}_{-0.07\ -0.02}$
5300	0.068	31	0.3	$0.53 \pm 0.10^{+0.07}_{-0.08}$
5300	0.130	47	0.1	$0.72 \pm 0.11^{+0.02}_{-0.01}$
5300	0.240	19	0.0	$0.29 \pm 0.07^{+0.01}_{-0.01}$
5300	0.420	19	0.0	$0.33 \pm 0.07^{+0.02}_{-0.02}$
9500	0.130	35	0.2	$0.67 \pm 0.11^{+0.03}_{-0.04}$
9500	0.240	40	0.0	$0.64 \pm 0.10^{+0.02}_{-0.03}$
9500	0.420	15	0.0	$0.25 \pm 0.06^{+0.02}_{-0.01}$
17000	0.240	19	0.1	$0.44 \pm 0.10^{+0.03}_{-0.03}$
17000	0.420	8	0.0	$0.15^{+0.08\ +0.01}_{-0.05\ -0.01}$
30000	0.420	5	0.0	$0.14^{+0.09\ +0.02}_{-0.06\ -0.02}$

Table 2: *Values of the reduced cross section. The following quantities are given: the values of Q^2 and x at which the cross section is quoted; the number of data events, N_{DATA}; the number of expected background events, N_{BG} and the measured cross section, with statistical and systematic uncertainties.*

$d\sigma/dQ^2$							
Q^2 (GeV^2)	$d\sigma/dQ^2$ (pb/ GeV^2)	δ_{stat} (%)	δ_{sys} (%)	δ_{unc} (%)	δ_1 (%)	δ_2 (%)	δ_3 (%)
280	$2.51 \cdot 10^{-2}$	± 25	$^{+21}_{-18}$	$^{+20}_{-18}$	$^{+5.1}_{-0.6}$	$^{+2.3}_{+5.5}$	$^{-3.7}_{+3.7}$
530	$2.70 \cdot 10^{-2}$	± 18	$^{+13}_{-16}$	$^{+10}_{-13}$	$^{-1.3}_{-3.4}$	$^{-1.5}_{-4.1}$	$^{-8.0}_{+8.0}$
950	$2.13 \cdot 10^{-2}$	± 11	$^{+6.0}_{-5.9}$	$^{+4.0}_{-4.7}$	$^{+3.4}_{-1.7}$	$^{-0.7}_{+0.4}$	$^{-3.0}_{+3.0}$
1700	$1.22 \cdot 10^{-2}$	± 8.8	$^{+3.4}_{-3.6}$	$^{+2.5}_{-2.9}$	$^{+0.0}_{-0.3}$	$^{+0.2}_{+0.7}$	$^{-2.1}_{+2.1}$
3000	$6.32 \cdot 10^{-3}$	± 8.6	$^{+2.0}_{-2.6}$	$^{+1.5}_{-2.5}$	$^{+0.7}_{+0.0}$	$^{+1.0}_{-0.3}$	$^{-0.6}_{+0.6}$
5300	$2.88 \cdot 10^{-3}$	± 9.3	$^{+3.5}_{-3.7}$	$^{+1.2}_{-2.1}$	$^{-0.7}_{+1.3}$	$^{+0.2}_{+0.2}$	$^{+3.0}_{-3.0}$
9500	$1.24 \cdot 10^{-3}$	± 11	$^{+3.3}_{-4.4}$	$^{+0.9}_{-2.8}$	$^{-3.0}_{+2.9}$	$^{+0.3}_{-1.1}$	$^{+1.2}_{-1.2}$
17000	$2.37 \cdot 10^{-4}$	± 18	$^{+6.7}_{-5.5}$	$^{+2.6}_{-1.2}$	$^{-5.3}_{+5.9}$	$^{-0.5}_{+1.6}$	$^{+0.4}_{-0.4}$
30000	$2.68 \cdot 10^{-5}$	$^{+55}_{-37}$	$^{+11}_{-13}$	$^{+0.8}_{-5.4}$	$^{-11}_{+11}$	$^{-5.5}_{+2.6}$	$^{+1.9}_{-1.9}$
$d\sigma/dx$							
x	$d\sigma/dx$ (pb)	δ_{stat} (%)	δ_{sys} (%)	δ_{unc} (%)	δ_1 (%)	δ_2 (%)	δ_3 (%)
0.015	$6.08 \cdot 10^{2}$	± 18	$^{+10}_{-9.1}$	$^{+8.5}_{-9.1}$	$^{+4.9}_{-0.9}$	$^{+2.5}_{-0.3}$	$^{-0.1}_{+0.1}$
0.032	$4.23 \cdot 10^{2}$	± 11	$^{+5.2}_{-7.7}$	$^{+2.6}_{-6.3}$	$^{+1.0}_{-0.7}$	$^{+0.9}_{+0.1}$	$^{-4.3}_{+4.3}$
0.068	$2.76 \cdot 10^{2}$	± 7.8	$^{+1.7}_{-2.6}$	$^{+1.6}_{-2.6}$	$^{+0.4}_{-0.4}$	$^{+0.1}_{+0.0}$	$^{-0.3}_{+0.3}$
0.130	$1.87 \cdot 10^{2}$	± 7.8	$^{+2.2}_{-1.4}$	$^{+1.2}_{-0.6}$	$^{-0.2}_{+1.2}$	$^{-0.8}_{+1.0}$	$^{+1.0}_{-1.0}$
0.240	$8.08 \cdot 10^{1}$	± 8.9	$^{+2.3}_{-2.1}$	$^{+1.6}_{-1.5}$	$^{-1.3}_{+1.3}$	$^{-0.2}_{+0.4}$	$^{-0.8}_{+0.8}$
0.420	$2.48 \cdot 10^{1}$	± 14	$^{+5.8}_{-4.1}$	$^{+2.1}_{+0.6}$	$^{-3.6}_{+4.9}$	$^{+2.2}_{-1.8}$	$^{-0.2}_{+0.2}$
0.650	$1.28 \cdot 10^{0}$	$^{+137}_{-67}$	$^{+15}_{-13}$	$^{+4.6}_{-2.6}$	$^{-12}_{+13}$	$^{+5.8}_{-4.1}$	$^{+0.8}_{-0.8}$
$d\sigma/dy$							
y	$d\sigma/dy$ (pb)	δ_{stat} (%)	δ_{sys} (%)	δ_{unc} (%)	δ_1 (%)	δ_2 (%)	δ_3 (%)
0.05	$1.40 \cdot 10^{2}$	± 12	$^{+8.7}_{-1.9}$	$^{+8.6}_{-1.8}$	$^{+1.1}_{-0.4}$	$^{-0.4}_{+0.9}$	$^{+0.1}_{-0.1}$
0.15	$1.18 \cdot 10^{2}$	± 8.4	$^{+4.0}_{-3.9}$	$^{+1.8}_{-2.2}$	$^{+0.6}_{+0.3}$	$^{+1.0}_{+0.5}$	$^{-3.3}_{+3.3}$
0.27	$8.85 \cdot 10^{1}$	± 8.2	$^{+2.9}_{-4.9}$	$^{+1.5}_{-3.3}$	$^{-0.8}_{-0.3}$	$^{-0.2}_{-2.4}$	$^{-2.5}_{+2.5}$
0.41	$5.63 \cdot 10^{1}$	± 10	$^{+3.6}_{-2.7}$	$^{+2.8}_{-2.6}$	$^{-0.1}_{+1.0}$	$^{+1.9}_{+0.3}$	$^{-0.8}_{+0.8}$
0.55	$5.40 \cdot 10^{1}$	± 11	$^{+3.3}_{-3.6}$	$^{+2.7}_{-3.0}$	$^{-0.1}_{-0.3}$	$^{+0.3}_{-0.7}$	$^{+1.8}_{-1.8}$
0.69	$5.07 \cdot 10^{1}$	± 12	$^{+3.7}_{-5.9}$	$^{+2.5}_{-4.7}$	$^{-1.9}_{+1.6}$	$^{-2.3}_{+1.4}$	$^{+1.8}_{-1.8}$
0.83	$3.01 \cdot 10^{1}$	± 18	$^{+12}_{-9.9}$	$^{+5.8}_{-8.3}$	$^{-2.3}_{+5.7}$	$^{-1.7}_{+6.7}$	$^{+4.6}_{-4.6}$

Table 3: *Values of the differential cross-sections $d\sigma/dQ^2$, $d\sigma/dx$ and $d\sigma/dy$. The following quantities are given: the value at which the cross section is quoted; the measured cross section; the statistical uncertainty; the total systematic uncertainty; the uncorrelated systematic uncertainty and those systematic uncertainties with significant (assumed 100%) correlations between cross-section bins. The systematic uncertainties considered to be correlated were: the first estimate of the calorimeter energy-scale uncertainty (δ_1); the second such estimate (δ_2) (see text); and the uncertainty in the parton-shower scheme(δ_3).*

Q^2 (GeV^2)	x	$\tilde{\sigma}$	δ_{stat} (%)	δ_{sys} (%)	δ_{unc} (%)	δ_1 (%)	δ_2 (%)	δ_3 (%)
280	0.032	0.64	$^{+57}_{-39}$	$^{+21}_{-9.6}$	$^{+18}_{-9.3}$	$^{+5.7}_{+0.1}$	$^{-1.4}_{+7.1}$	$^{-1.4}_{+1.4}$
530	0.015	1.13	$^{+43}_{-32}$	$^{+13}_{-23}$	$^{+12}_{-22}$	$^{+5.1}_{-1.2}$	$^{-3.5}_{-6.8}$	$^{-2.0}_{+2.0}$
530	0.032	0.91	$^{+39}_{-29}$	$^{+8.8}_{-18}$	$^{+3.1}_{-15}$	$^{-1.1}_{-0.2}$	$^{+2.4}_{-4.5}$	$^{-7.9}_{+7.9}$
530	0.068	0.83	$^{+50}_{-35}$	$^{+17}_{-22}$	$^{+11}_{-17}$	$^{-5.7}_{-4.5}$	$^{-2.5}_{+1.6}$	$^{-13}_{+13}$
950	0.015	1.51	± 26	$^{+17}_{-19}$	$^{+16}_{-17}$	$^{+5.9}_{-5.1}$	$^{-2.8}_{-4.0}$	$^{-0.8}_{+0.8}$
950	0.032	0.75	± 25	$^{+11}_{-11}$	$^{+6.3}_{-9.7}$	$^{+4.6}_{-1.1}$	$^{+3.6}_{+3.8}$	$^{-5.1}_{+5.1}$
950	0.068	1.01	± 19	$^{+12}_{-13}$	$^{+9.5}_{-8.7}$	$^{+0.3}_{-4.0}$	$^{-2.7}_{-2.2}$	$^{-8.0}_{+8.0}$
950	0.130	0.79	± 25	$^{+14}_{-11}$	$^{+8.0}_{-4.8}$	$^{+4.2}_{+3.3}$	$^{-1.9}_{+2.2}$	$^{+9.6}_{-9.6}$
1700	0.032	0.87	± 18	$^{+13}_{-5.8}$	$^{+12}_{-5.6}$	$^{+0.7}_{+1.9}$	$^{+2.6}_{+2.0}$	$^{-1.4}_{+1.4}$
1700	0.068	0.81	± 14	$^{+2.6}_{-5.9}$	$^{+1.8}_{-5.4}$	$^{+0.7}_{-1.0}$	$^{+0.5}_{-1.4}$	$^{-1.7}_{+1.7}$
1700	0.130	0.75	± 18	$^{+3.5}_{-6.3}$	$^{+1.3}_{-4.9}$	$^{-0.3}_{-1.8}$	$^{-1.3}_{+0.2}$	$^{-3.3}_{+3.3}$
1700	0.240	0.47	± 24	$^{+2.7}_{-4.8}$	$^{+1.1}_{-3.0}$	$^{-1.2}_{-0.3}$	$^{-2.9}_{+1.3}$	$^{-2.1}_{+2.1}$
3000	0.068	0.71	± 14	$^{+6.3}_{-1.9}$	$^{+4.7}_{-0.3}$	$^{+2.5}_{+1.6}$	$^{+2.1}_{+1.1}$	$^{-1.9}_{+1.9}$
3000	0.130	0.58	± 17	$^{+5.9}_{-3.7}$	$^{+4.9}_{-2.3}$	$^{+1.0}_{-0.1}$	$^{+0.9}_{+0.7}$	$^{+2.9}_{-2.9}$
3000	0.240	0.49	± 19	$^{+1.7}_{-3.0}$	$^{+0.9}_{-2.4}$	$^{-0.5}_{-0.6}$	$^{+0.5}_{-0.8}$	$^{-1.4}_{+1.4}$
3000	0.420	0.21	$^{+49}_{-35}$	$^{+11}_{-9.8}$	$^{+8.9}_{-9.7}$	$^{-0.9}_{+5.6}$	$^{+2.5}_{+0.2}$	$^{+1.5}_{-1.5}$
5300	0.068	0.53	± 18	$^{+13}_{-15}$	$^{+3.6}_{-7.5}$	$^{-2.1}_{+0.1}$	$^{-1.7}_{+1.1}$	$^{+12}_{-12}$
5300	0.130	0.72	± 15	$^{+2.7}_{-1.1}$	$^{+1.5}_{-1.1}$	$^{+0.1}_{+1.7}$	$^{+0.1}_{+1.3}$	$^{+0.0}_{-0.0}$
5300	0.240	0.29	± 23	$^{+2.8}_{-5.1}$	$^{+1.7}_{-4.9}$	$^{+0.2}_{+1.6}$	$^{+1.5}_{-1.2}$	$^{-0.5}_{+0.5}$
5300	0.420	0.33	± 23	$^{+6.0}_{-6.2}$	$^{+2.3}_{-2.8}$	$^{-1.0}_{+2.3}$	$^{+2.5}_{-3.2}$	$^{-4.4}_{+4.4}$
9500	0.130	0.67	± 17	$^{+3.8}_{-6.2}$	$^{+1.4}_{-4.9}$	$^{-3.3}_{+3.5}$	$^{-2.0}_{+0.2}$	$^{+0.0}_{-0.0}$
9500	0.240	0.64	± 16	$^{+2.4}_{-4.7}$	$^{+0.4}_{-3.6}$	$^{-2.3}_{+1.1}$	$^{+1.1}_{-1.1}$	$^{+1.8}_{-1.8}$
9500	0.420	0.25	± 26	$^{+6.3}_{-5.1}$	$^{+2.5}_{-0.4}$	$^{-3.5}_{+3.9}$	$^{+4.1}_{-3.5}$	$^{-0.9}_{+0.9}$
17000	0.240	0.44	± 23	$^{+7.1}_{-6.1}$	$^{+2.7}_{-1.6}$	$^{-5.0}_{+4.8}$	$^{-3.1}_{+4.3}$	$^{-0.9}_{+0.9}$
17000	0.420	0.15	$^{+50}_{-35}$	$^{+9.6}_{-7.3}$	$^{+3.1}_{-1.3}$	$^{-4.9}_{+6.2}$	$^{+6.2}_{-4.6}$	$^{+2.3}_{-2.3}$
30000	0.420	0.14	$^{+68}_{-43}$	$^{+13}_{-13}$	$^{+1.8}_{-5.4}$	$^{-9.4}_{+10}$	$^{-5.9}_{+5.1}$	$^{+5.3}_{-5.3}$

Table 4: *Values of the reduced cross section. The following quantities are given: the values of Q^2 and x at which the cross section is quoted; the measured cross section; the statistical uncertainty; the total systematic uncertainty; the uncorrelated systematic uncertainty and those systematic uncertainties with significant (assumed 100%) correlations between cross-section bins. The systematic uncertainties considered to be correlated were: the first estimate of the calorimeter energy-scale uncertainty (δ_1); the second such estimate (δ_2) (see text); and the uncertainty in the parton-shower scheme(δ_3).*

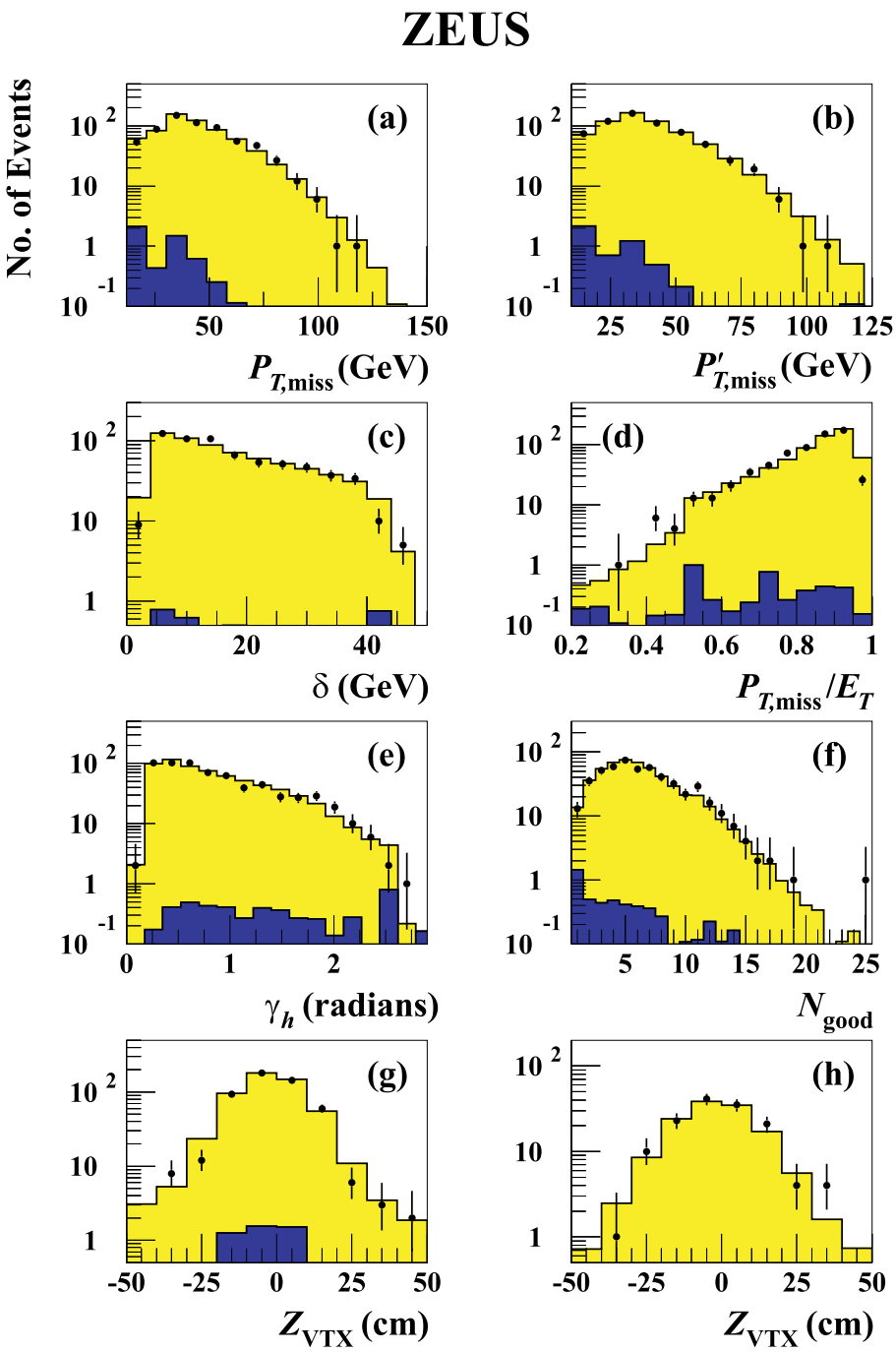

Figure 1: *Comparison of the final e^-p CC data sample (solid points) with the expectations of the sum of the signal and ep background Monte Carlo simulations (light shaded histogram). The ep background Monte Carlo is shown as the dark shaded histogram. (a) the missing transverse momentum, $P_{T,\mathrm{miss}}$, (b) $P_{T,\mathrm{miss}}$ excluding the very forward cells, $P'_{T,\mathrm{miss}}$, (c) the variable δ, defined in the text, (d) the ratio of missing transverse momentum to total transverse energy, $P_{T,\mathrm{miss}}/E_T$, (e) γ_h, (f) the number of good tracks, (g) the Z position of the CTD vertex for the high-γ_0 sample and (h) the Z position of the timing vertex for the low-γ_0 sample.*

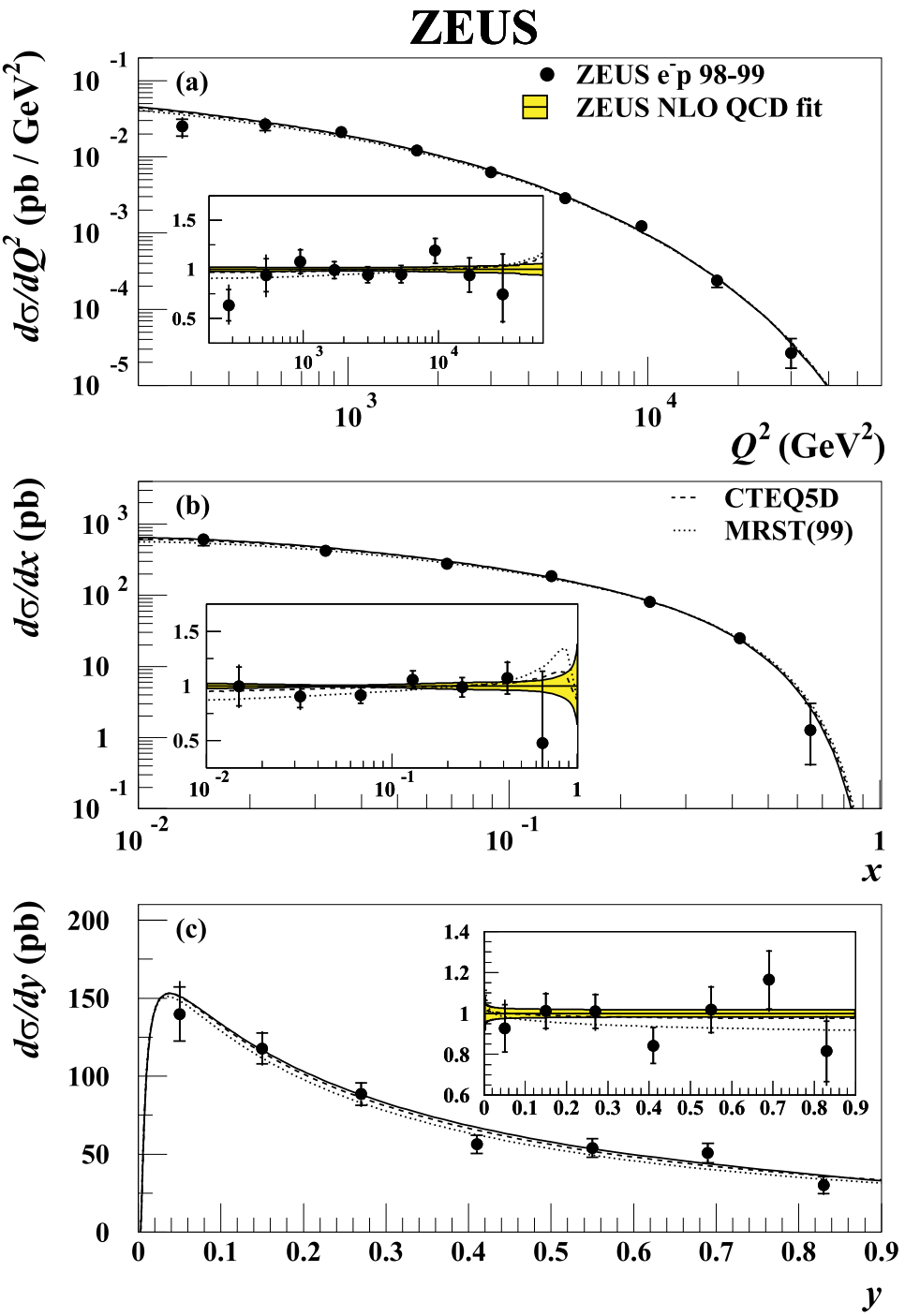

Figure 2: *The e^-p CC DIS cross-sections (a) $d\sigma/dQ^2$, (b) $d\sigma/dx$ and (c) $d\sigma/dy$ for data (solid points) and the SM expectation evaluated using the ZEUS NLO QCD fit, CTEQ5D and MRST(99) PDFs. The insets show the ratios of the measured cross sections to the SM expectations evaluated using the ZEUS NLO QCD fit. The statistical errors are indicated by the inner error bars (delimited by horizontal lines), while the full error bars show the total uncertainty obtained by adding the statistical and systematic contributions in quadrature. The shaded band shows the uncertainties associated with the PDFs estimated using the ZEUS NLO QCD fit.*

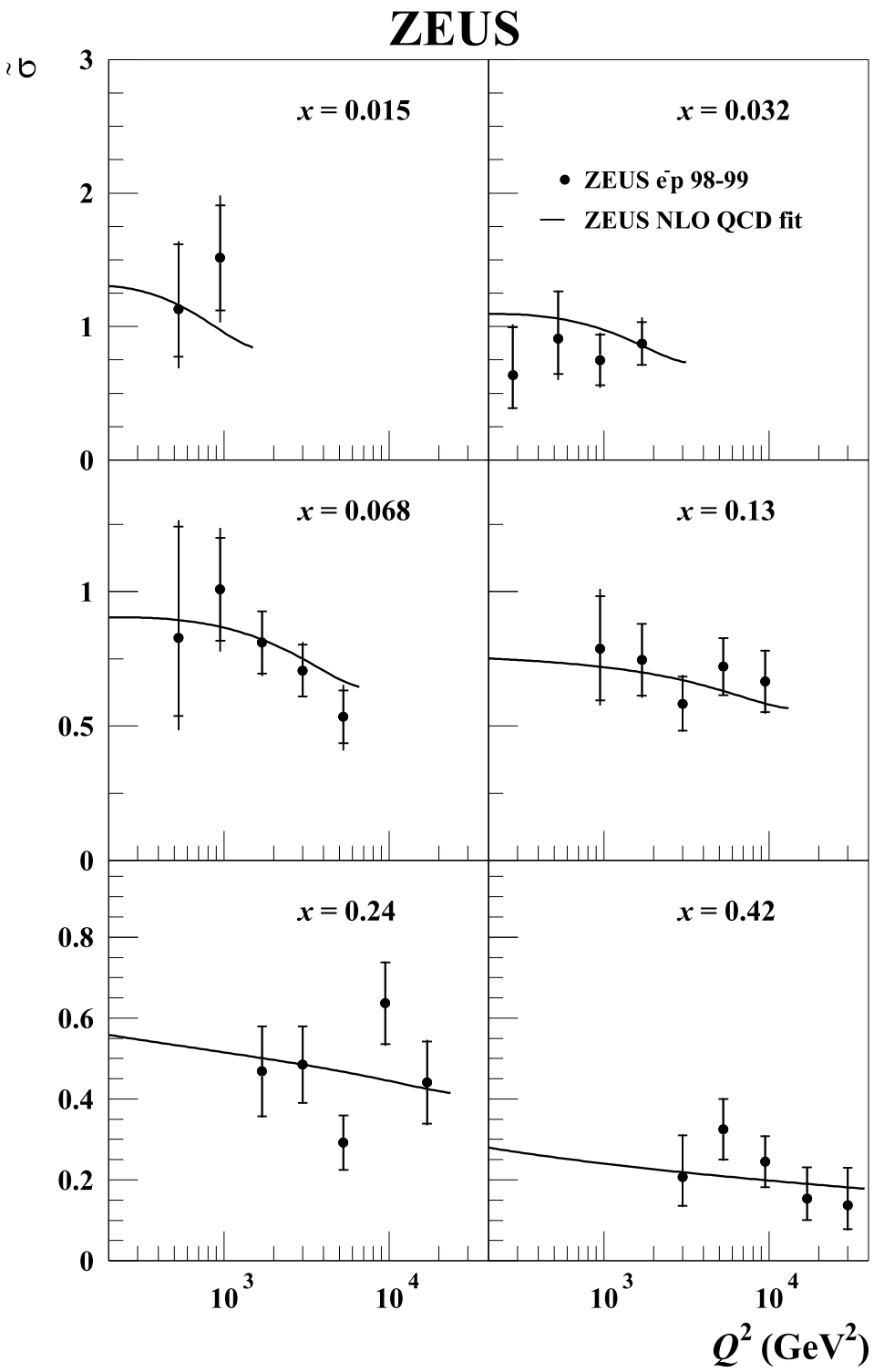

Figure 3: *The reduced cross section, $\tilde{\sigma}$, as a function of Q^2, for different fixed values of x. The points represent the data, while the expectation of the Standard Model evaluated using the ZEUS NLO QCD fit is shown as a line.*

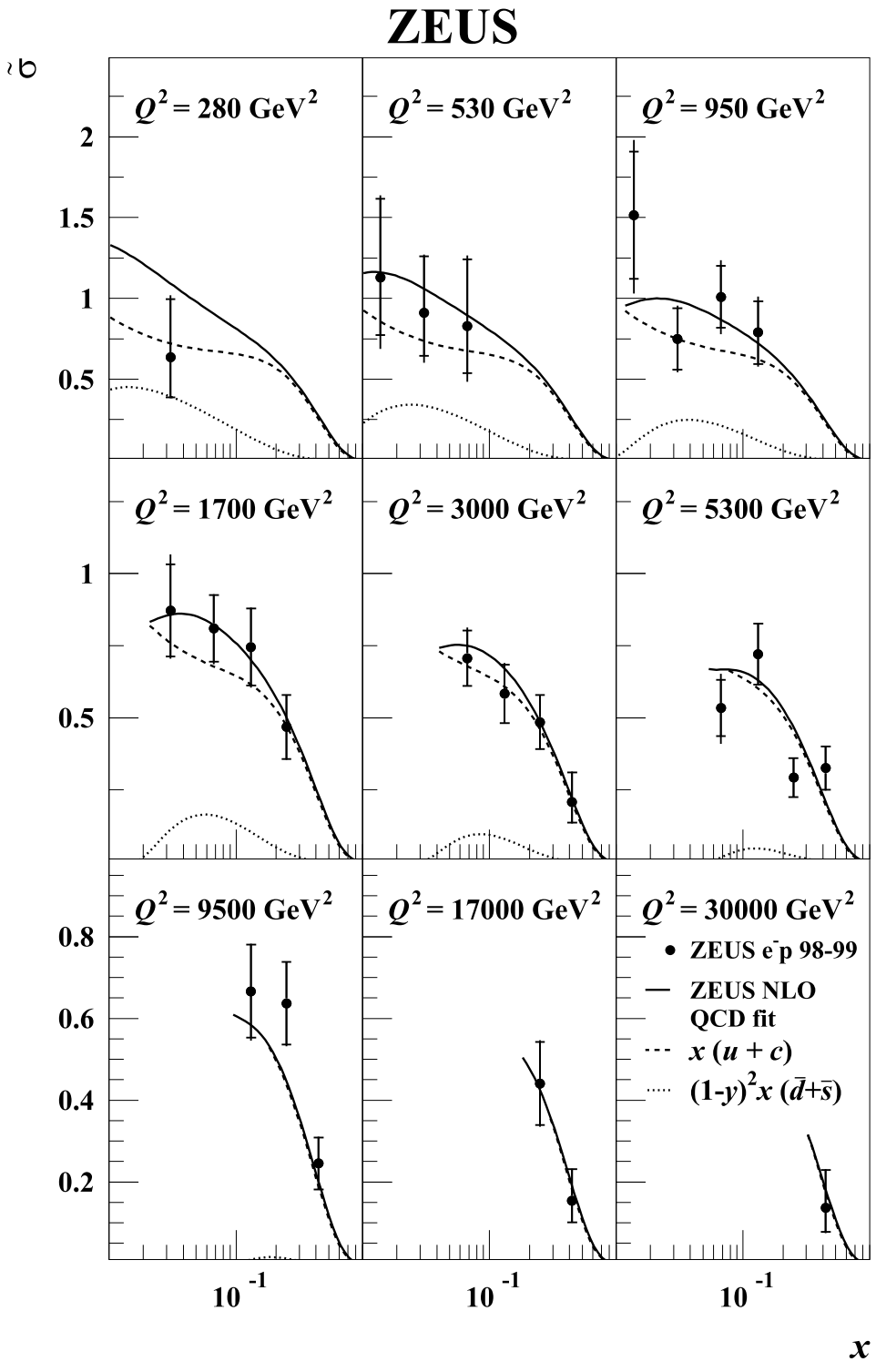

Figure 4: *The reduced cross section, $\tilde{\sigma}$, as a function of x, for different values of Q^2. The points represent the data, while the expectation of the Standard Model evaluated using the ZEUS NLO QCD fit is shown as a solid line. The separate contributions of the PDF combinations $x(u+c)$ and $(1-y)^2 x(\bar{d}+\bar{s})$ are shown by the dashed and dotted lines, respectively.*

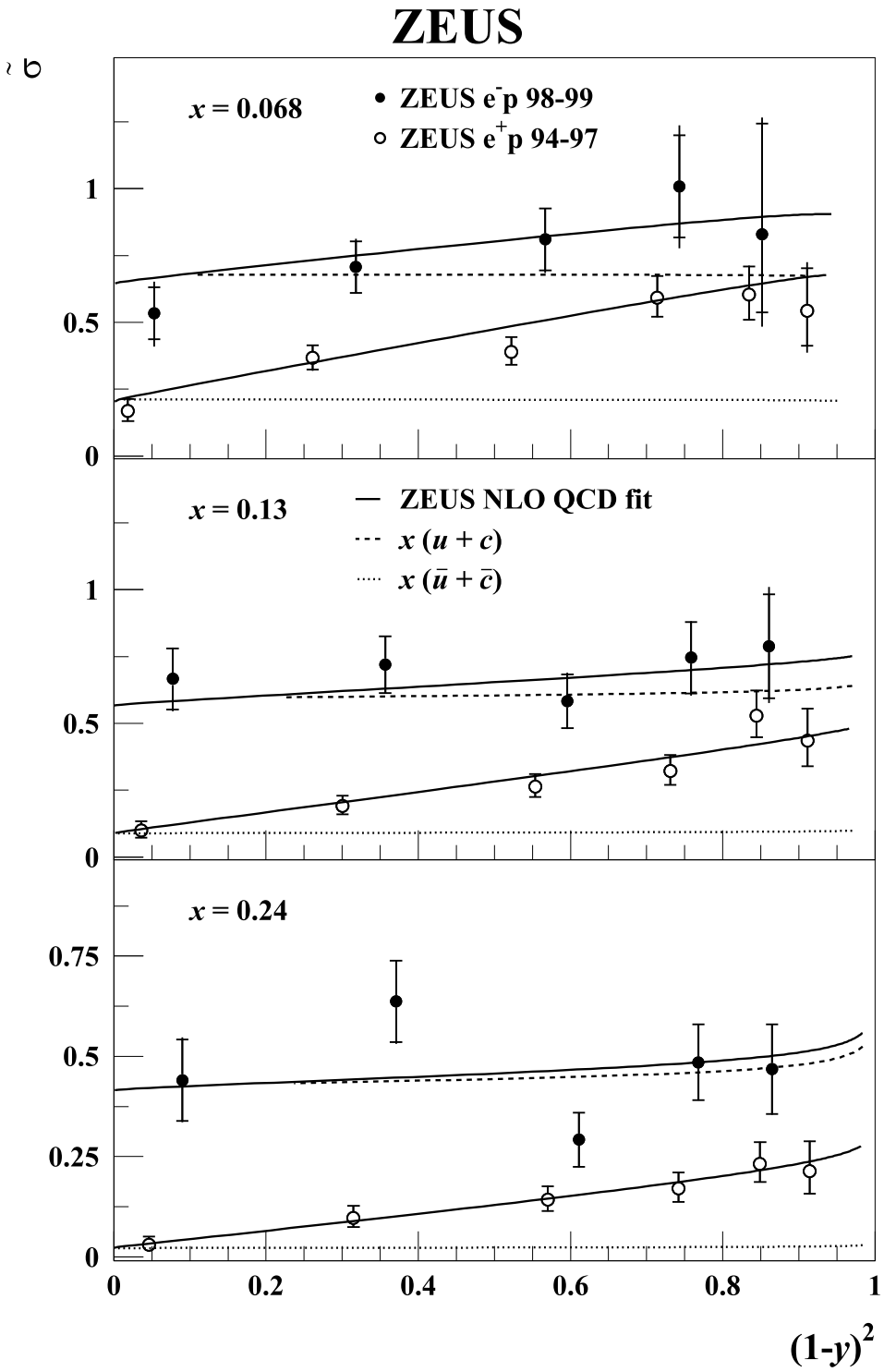

Figure 5: *The reduced cross section, $\tilde{\sigma}$, as a function of $(1-y)^2$, for different fixed values of x, for e^-p (solid points) and e^+p (open circles) CC DIS. The expectation of the Standard Model evaluated using the ZEUS NLO QCD fit is shown as a solid line. The contributions of the PDF combinations $x(u+c)$ and $x(\bar{u}+\bar{c})$ are shown by the dashed and dotted lines, respectively.*